



HAL
open science

Drawing Nanocomposite Optical Fibers: Shaping Particles and Bubbles

Manuel Vermillac, Francois Peters, Courtney Kucera, T W Hawkins, John
Ballato, Wilfried Blanc

► **To cite this version:**

Manuel Vermillac, Francois Peters, Courtney Kucera, T W Hawkins, John Ballato, et al.. Drawing Nanocomposite Optical Fibers: Shaping Particles and Bubbles. Sensors & Transducers., 2018. hal-01985832

HAL Id: hal-01985832

<https://hal.science/hal-01985832>

Submitted on 18 Jan 2019

HAL is a multi-disciplinary open access archive for the deposit and dissemination of scientific research documents, whether they are published or not. The documents may come from teaching and research institutions in France or abroad, or from public or private research centers.

L'archive ouverte pluridisciplinaire **HAL**, est destinée au dépôt et à la diffusion de documents scientifiques de niveau recherche, publiés ou non, émanant des établissements d'enseignement et de recherche français ou étrangers, des laboratoires publics ou privés.

Drawing Nanocomposite Optical Fibers: Shaping Particles and Bubbles

¹ Manuel VERMILLAC, ¹ François PETERS, ² Courtney KUCERA,
² Thomas W. HAWKINS, ² John BALLATO and ^{1,*} Wilfried BLANC

¹ Université Côte d'Azur, Institut de Physique de Nice, CNRS UMR 7010, Parc Valrose, Nice, France

² Center for Optical Materials Science and Engineering Technologies (COMSET) and the Department of Materials Science and Engineering, Clemson University, Clemson, South Carolina 29634 USA

¹ Tel.: +33 4 92 07 67 99, fax: +33 4 92 07 67 54

* E-mail: wilfried.blanc@unice.fr

Received: 25 June 2018 / Accepted: 31 August 2018 / Published: 31 October 2018

Abstract: Optical fibers are the basis for applications that have grown considerably in recent years (telecommunications, sensors, fiber lasers, etc.). To fulfill the characteristics required for these applications, optical fibers are obtained by drawing high-purity silica-based preforms. This drawing step is usually assumed to be a homothetic transformation of the preform. However, at this stage, the glass is heated at temperature higher than its softening temperature. Then the glass flows which can induce the transformation of heterogeneities. In this paper, we highlight the elongation of bubbles and even break up of oxide nanoparticles during the drawing process. These phenomena allow new routes to optical fibers with light transport induced by transverse Anderson localization of light or new amplifying properties.

Keywords: Optical fibers, Drawing, Nanoparticles, Bubbles.

1. Introduction

Optical fibers are now part of everyday technologies, usually associated with telecommunications and high-speed internet [1]. Far from being confined to this single use, optical fibers are deployed in many fields of applications, especially as sensors (strain, temperature, pressure, etc.) for over 40 years [2].

Usually, the design of these fibers is based on a homogeneous composition of the core, which can be locally structured at a microscale in the case of the fiber Bragg grating. In this article, we will discuss about an emerging class of optical fibers which contain heterogeneities such as oxide nanoparticles to improve luminescence properties or air bubbles to tailor light guiding properties [3].

These key applications rely on the qualities of silica glass: mechanical and chemical stability, high optical damage threshold, low cost, etc. To fulfill the characteristics required for these applications, many processes have been developed to prepare high purity silica-based preforms: MCVD (Modified Chemical Vapor Deposition) [4], OVD (Outside Vapor Deposition) [5], VAD (Vapor Axial Deposition) [6], DND (Direct Nanoparticle Deposition) [7], Rod-in-tube and powder in tube [8]. Usually, these processes aim at preparing homogeneous preforms in the longitudinal direction in order to prepare many kilometers of fiber with constant opto-geometrical characteristics. Indeed, during the process of optical fiber fabrication, the drawing step could be considered as a homothetic transformation of the transverse section from the preform to the fiber: same core

diameter/external diameter ratio and same refractive index profile. However, during the drawing step, the glass is heated at ~ 2000 °C, which is above its softening temperature (typically 1650 °C for silica), and quenched within few seconds. From a macroscopic point of view, this high quenching rate leads to residual stress which is known to affect optical properties such as the refractive index profile [9]. From a microscopic point of view, structural modifications were also reported such as preferential orientation of small-sized silica rings [10]. During this presentation, we will discuss about the effects of the drawing step on the shape of the particles and bubbles.

2. Elongation and Breakup of Particles

Various luminescent-based optical fiber sensors have been reported for optical thermometry [11]. To develop intrinsic fiber optic temperature sensor, one route of interest relies on the doping with rare-earth ions. H. Bertou and C.K. Jörgensen were the first to report on the ability to measure temperature in fluoride fiber doped with erbium (Er^{3+}) ions, sensitized by ytterbium (Yb^{3+}) ions [12]. With these fibers, the temperature is determined by measuring the intensity ratio of two green emissions of Er^{3+} ions (520 and 550 nm emission bands). Moreover, as fiber lasers, rare-earth doped fibers are also key components as light sources for numerous applications such as remote sensing (LIDAR), or as transducers when coupled with Bragg gratings [13].

The luminescence properties of rare earth ions are linked to their electronic structure. The optically active electrons belong to their f -shell, offering most of the electronic transitions of interest for optical fiber applications (like the $^4\text{I}_{13/2} \rightarrow ^4\text{I}_{15/2}$ emission transition of Er^{3+} at 1.5 μm or the $^2\text{F}_{5/2} \rightarrow ^2\text{F}_{7/2}$ transition for Yb^{3+} main emission around 1 μm). The spectroscopic properties of these luminescent ions (oscillator strengths, energy of the electronic levels, electron-phonon coupling, etc.) strongly depend on the arrangement and the nature of the surrounding atoms [14].

Silica glass as a fiber host material has proved to be very attractive for developing efficient fiber amplifiers and high-power fiber lasers [15]. While this glass offers many advantages such as low optical losses, high reliability and low cost, it suffers from limitations in term of spectroscopic properties. Thus, the development of new active optical fiber devices requires materials with “augmented” intrinsic properties, though using luminescent ion-doped silica as host glass. Dielectric nanoparticles in optical fibers are thus considered as they can combine the sturdiness and low cost of silica with particular spectroscopic behavior that would not appear in a pure silica local-environment [16]. The nanoparticles would optimally fully encapsulate the rare-earth ions to produce “engineered” spectroscopic properties.

To investigate the role of the drawing step, we have prepared a MCVD-preform with a doping solution containing $\text{LaF}_3:\text{Tm}^{3+}$ nanoparticles. During the process, fluorine ions react and evaporate. As a consequence, the optical fiber preform contains La-rich silicate nanoparticles [17].

The preform was cut and polished in the longitudinal direction (*i.e.* along the drawing axis). Spherical nanoparticles were imaged thanks to scanning electron microscopy (SEM) measurements. After the drawing step, the morphology of the larger particles is altered. To illustrate this change, the nanoparticles were characterized by x-ray nanotomography. This technique has the ability to combine 2D or 3D visualization of the chemical contrast in a volume larger than the core size with a spatial resolution of a few tens of nanometers, commensurate with the size of the nanoparticles. An example of a 3D-reconstruction is presented in Fig. 1, which corresponds to the image of the overall core of the fiber over a length of 16.5 μm . The nanoparticles were colored based on their length: 0.05-0.35 μm in yellow, 0.35-10 μm in blue, and 10-16 μm in red. The blue sphere on the top of the picture corresponds to a gold bead used to improve the 3D-reconstruction. The glass surrounding the nanoparticles is not displayed. Following this procedure, it is clearly observed that nanoparticles in the fiber center lead to thicker elongated regions while those at the core periphery are thinner and experience greater Rayleigh-Plateau instability, which leads to the break-up of the thread into smaller nanoparticles.

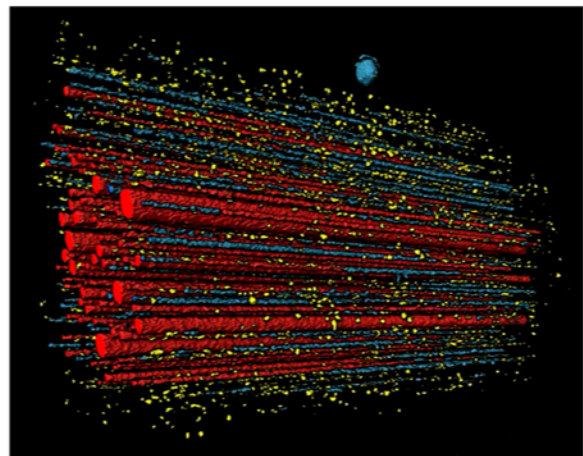


Fig. 1. X-ray nanotomography characterization of the fiber showing the distribution of the nanoparticles as a function of their length. Colors coding is explained in the text. The field of view is 16.5 $\mu\text{m} \times 16.5 \mu\text{m} \times 16.5 \mu\text{m}$. The particles are aligned along the drawing axis.

The optical fiber containing La-rich silicate nanoparticles was etched with a Focus Ion Beam (FIB) to looking at a longitudinal section of the core with (SEM). Fig. 2 is the volume reconstruction of the core obtained by using a FIB/SEM tomography [18].

Particles with radius smaller than 10 nm and glass matrix surrounding particles are not plotted in Fig. 2. Particles can be sorted according to three sets:

- 1) Nanoparticles with diameter in the 10-40 nm range which are almost spherical;
- 2) Larger particles with long axes ranging from 65 nm to 230 nm;
- 3) Highly elongated particles.

According to x-ray nanotomography analyses, the length of these elongated particles can be as long as 300 μm .

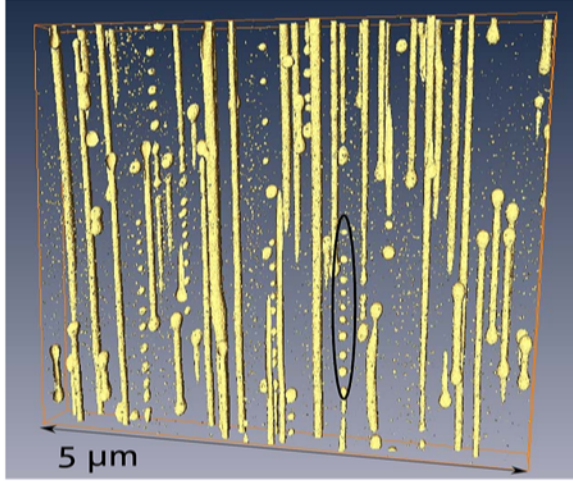


Fig. 2. Partial volume reconstruction of the core of the optical fiber imaged by FIB and SEM. Nanoparticles induced by Rayleigh-Plateau instability are circled. The drawing direction is vertical.

From rheology of emulsion and polymers, it is known that the deformation of particles is induced by the competition between the viscous stresses on particles and the surface tension. The study of the deformation is based on the capillary number (Ca):

$$Ca = \frac{\sigma R}{\gamma}, \quad (1)$$

where γ is the surface tension, σ the viscous stress from the flow and R the radius of particles. The viscous stress (σ) is expressed as:

$$\sigma = 3 \times \eta \times \dot{\epsilon}, \quad (2)$$

where η is the viscosity of the matrix and $\dot{\epsilon}$ is its deformation rate.

It is reported that if $Ca < Ca_c$ (Ca_c is the critical capillary number), an ellipsoidal stationary shape exists, if $Ca > Ca_c$ the particle elongates into a long cylinder until it breaks due to Rayleigh instabilities or until viscous stresses are decreased.

Based on this approach, we can interpret the sets of particles observed in Fig. 2. Long elongated particles (cylinders) are present because the flow was not

maintained long enough to initiate break up. It would need more deformation to reduce their diameters and to amplify the instabilities. When the amplitude of growing instabilities is comparable to the radius of the cylinder, the cylinder can break up. It is evidenced by the presence of particles with the same size, periodically spaced and aligned in the direction of the flow (particles circled in Fig. 2). These newly formed particles and particles smaller than 40 nm can not break up (under this drawing conditions) because $Ca < Ca_c$. Then, the break up of initial large particles is restricted to a range of diameters. The deformation can be quantified using the Taylor parameter D :

$$D = \frac{L - B}{L + B}, \quad (3)$$

where L and B are the major (larger) and minor (small) axes of the (ellipsoidal-like) elongated particle, respectively. Particles longer than 300 μm are observed, leading to a deformation higher than 0.99 (the radius is estimated to be about 250 nm). Considering their high elongation, break-up is not achieved due to quenching of the glass, which ceases any further deformation.

These phenomena clearly offer new possibilities for the control of the size and shape of particles. These observations are of a great interest for light scattering issues as they allow to reduce the size of the particles in the final fiber.

3. Influence of the Drawing Temperature

In order to study the effect of the drawing temperature, a MCVD preform was prepared with a doping solution containing LaCl_3 and ErCl_3 chlorides salts dissolved in ethanol. This fiber was drawn at three different temperatures: 1950, 1810 and 1795 $^\circ\text{C}$, corresponding to three drawing tensions: 0.3, 1.5 and 2 N, respectively. The SEM images are shown in Fig. 3. While elongated particles are present in all images, the main difference relates to the fragmented particles. Indeed, in the 0.3, 1.5 and 2 N drawn fibers, the number of fragmentation-induced particles was estimated to be around 110, 1200 and 2500, respectively (areas investigated were the same for all the fiber cores).

When the capillary number increases (higher than the critical capillary number), particles that elongate enough undergo Rayleigh-Plateau instability during fiber drawing, which can induce break-up. This phenomenon has been observed also when drawing a composite fiber made of chalcogenide glass [19] or metal [20] core embedded in a polymer cladding. The break-up produces chains of homogeneously spaced particles with monodispersed diameters, as observed in Fig. 3. In this and the Author's previous work, it has been observed that increasing drawing tension (decreasing drawing temperature) favors break-up. This can be explained by the increase of the capillary

number [21]. Indeed, for a particle of defined radius, the higher the drawing tension, hence viscous stress, then the higher the capillary number (cf Equation (1)).

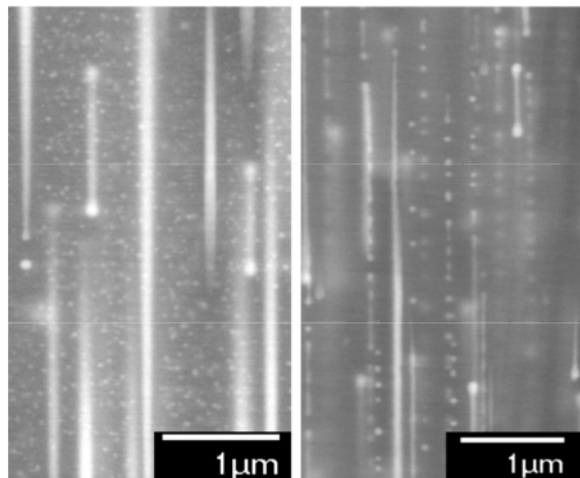


Fig. 3. SEM images (back-scattered electrons) of fiber drawn at different drawing temperatures: 1950 and 1795°C (corresponding to different drawing tensions: 0.3 and 2 N, respectively), from left to right. The drawing axis is horizontal.

4. Elongation of Bubbles

Air-bubbles containing optical fibers have been studied for many applications thanks to their ability to tailor light guiding properties. In conventional optical fibers, light is guided in the core due to its higher refractive index compare to the one of the surrounding cladding. To increase the refractive index difference, D. Kominsky, *et al.* have proposed a *random-hole fiber* [22]. In this holey optical fiber, the holes are located in the cladding. Then, the air-silica fraction allows to determine the refractive index. It has been reported also that air-bubbles containing optical fibers have interest as ultra-low bending loss single mode fiber, endless single mode optical fiber and light diffusing fiber [23].

Recently, a new route to light transport was demonstrated and is based on transverse Anderson localization of light in an optical fiber with transverse refractive index fluctuations [24]. The Anderson localized fiber allowed for the simultaneous propagation of multiple beams in a single strand of disordered optical fiber with potential applications in optical, biological and medical imaging, and beam-multiplexed optical communications. A directional random laser mediated by transverse Anderson localization in a disordered glass optical fiber was reported also [25]. With respect to sensing applications, beyond that aforementioned imaging uses, these random fiber lasers potentially offer low threshold, broad bandwidth light sources that emit over the cross-section of the fiber rather than just the small fiber core.

To obtain the transverse refractive index fluctuations, the starting preform was a ‘satin quartz’, which is a porous artisan silica glass. A transverse section of the preform imaged by SEM is presented in Fig. 4. In this image, the black dots correspond to the air bubbles which are homogeneously distributed all over the cross-section. In this transverse direction, the air-holes diameters vary between 10 and 100 μm. A piece of this preform has been polished in the longitudinal direction to image the air-holes. In the longitudinal direction, most of the air-holes are spherical or slightly elongated (Fig. 5). Only few air-holes have a high deformation value.

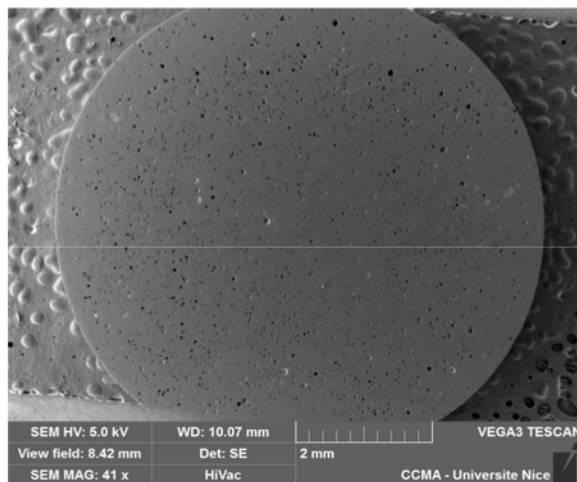


Fig. 4. SEM image of a preform (transverse section) containing air-holes.

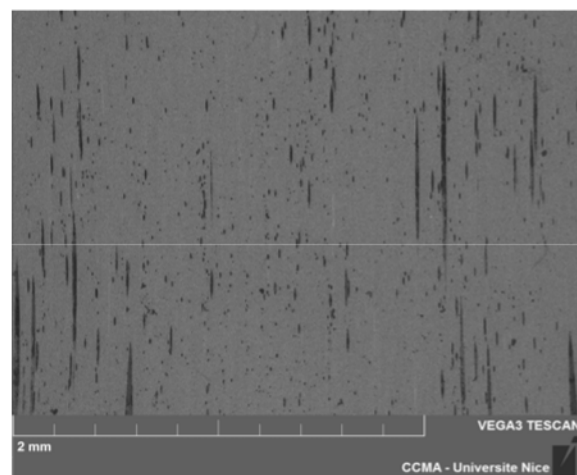


Fig. 5. SEM image of a preform (longitudinal direction) containing air-holes.

The preform has been drawn into optical fiber under normal conditions (drawing temperature = 2000 °C, drawing tension = 0.2 N). The diameter of the final fiber is ~ 250 μm and the average air fill-fraction is about 5.5 %. In the transverse section, the air-hole diameters vary between about 0.2

and 5.5 μm (Fig. 6). A piece of fiber was polished over 2 cm in the longitudinal section to image the elongation of the air-bubbles (Fig. 7). Note that due to the carbon coating, some of the air-channels are polluted, i.e. filled with carbon dust. The elongation of these air-bubbles over several millimeters was measured. This length is longer than the one of the elongated bubbles in the preform. It tends to prove the elongation of the air-bubbles during the drawing step. However, this measurement protocol could impact the true value of the elongation length. Indeed, to be able to detect a 4- μm air channel over 1 mm or 1 cm, the angle between the polished surface and the longitudinal axis of the fiber must be smaller than 0.2° and 0.02° , respectively (assuming a cylindrical shape for the air-channel).

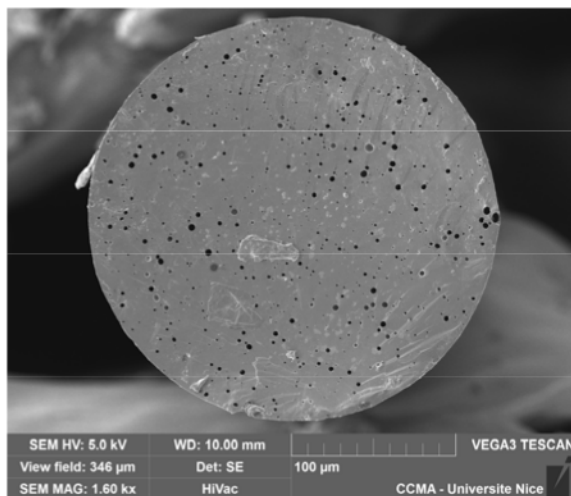


Fig. 6. SEM image of a fiber (transverse section) containing air-holes.

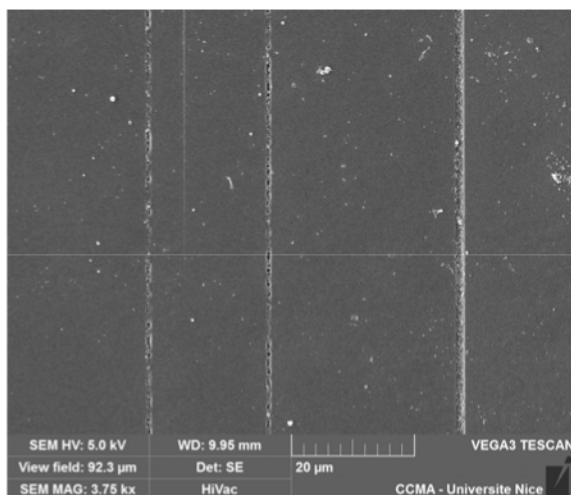


Fig. 7. SEM image of a fiber (longitudinal direction) with elongated bubbles.

It has been reported that the evolution of the air-bubbles during the drawing of the optical fiber

depends on many parameters such as the diffusivity of the gas in the glass, the heating history, and the initial starting distance between the air bubbles [23]. Then, closed bubbles or gas with high diffusivity would favor the coalescence of bubbles during the drawing step and change the features of the air-bubbles in the final fiber.

5. Conclusions

The drawing step is usually considered as a homothetic transformation from the preform to the fiber. However, the flow of the glass can be used to induce elongation of heterogeneities such as bubbles and even the break up of nanoparticles.

The influence of draw temperature (tension) on the morphology of oxide nanoparticles embedded in the core of silica optical fibers was studied. During the draw step, spherical particles present in the preform can undergo elongation and even break-up into smaller particles. Elongation is due to flow-induced deformation and Rayleigh-Plateau instabilities. In this work, particles as long as 300 μm have been reported. Moreover, this work demonstrates that it is possible to favor break-up phenomenon by decreasing draw temperature (increasing draw tension), which offers new opportunities to control and tailor the size and shape of active particles in optical fibers.

A change of the characteristics of air-holes is reported also. This would have some impact on the Anderson localized fiber which allow for the simultaneous propagation of multiple beams in a single strand of disordered optical fiber with potential applications in optical, biological and medical imaging, and beam-multiplexed optical communications.

Acknowledgements

This work is partly funded by Agence Nationale de la Recherche (ANR-14-CE07-0016-01, Nice-DREAM). We thank M. Cabie (CP2M, Marseille, France) and F. Orange (CCMA, Nice, France) for SEM images, and D. Boreschneck (CEREGE, Aix-en-Provence, France) for X-ray nanotomography characterizations.

References

- [1]. K. C. Kao, G. A. Hockham, Dielectric-fibre surface waveguides for optical frequencies, in *Proc. IEE*, Vol. 113, Issue 7, 1966, pp. 1151-1158.
- [2]. B. Lee, Review of the Present Status of Optical Fiber Sensors, *Optical Fiber Technology*, Vol. 9, Issue 2, 2003, pp. 57–79.
- [3]. W. Blanc, M. Vermillac, F. Peters, C. Kucera, M. A. Tuggle, T. W. Hawkins, J. Ballato, Drawing optical fibers: elongating bubbles, breaking nanoparticles, in *Proceeding of the 1st International Conference on*

- Optics, Photonics and Lasers (OPAL'18)*, Barcelona, Spain, 9-11 May 2018, pp. 77-80.
- [4]. J. B. MacChesney, P. B. O'Connor, H. M. Presby, A New Technique for the Preparation of Low-loss and Graded-index Optical Fibers, in *Proc. IEEE*, Vol. 62, Issue 9, 1974, pp. 1280-1281.
- [5]. D. B. Keck, P. C. Schultz, F. Zimar, Method of forming optical waveguide fibers, *US Patent 3,737,292*, 1973.
- [6]. T. Izawa, S. Kobayashi, S. Sudo, F. Hanawa, Continuous Fabrication of High Silica Fibre Preform, in *Proceeding of the International Conference on Integrated Optics and Optical-fibre Communication*, C1-1, 1977.
- [7]. S. Tammela, M. Söderlund, J. Koponen, V. Philippov, P. Stenius, The Potential of Direct Nanoparticle Deposition for the Next Generation of Optical Fibers, in *Optical Components and Materials III*, Vol. 6116, 2006, p. 61160G - 61160G-9.
- [8]. J. Ballato, E. Snitzer, Fabrication of fibers with high rare-earth concentrations for Faraday isolator applications, *Applied Optics*, Vol. 34, Issue 30, 1995, pp. 6848-6854.
- [9]. P. L. Chu, T. Whitbread, Measurement of stresses in optical fiber and preform, *Applied Optics*, Vol. 21, Issue 23, 1982, pp. 4241-4245.
- [10]. X. Bidault, S. Chaussdent, W. Blanc, D. R. Neuville, Deformation of silica glass studied by molecular dynamics: Structural origin of the anisotropy and non-Newtonian behavior, *Journal of Non-Crystalline Solids*, Vol. 433, 2016, pp. 38-44.
- [11]. M. McSherry, C. Fitzpatrick, E. Lewis, Review of luminescent based fibre optic temperature sensors, *Sensor Review*, Vol. 25, Issue 1, 2005, pp. 56-62.
- [12]. H. Bertou, C.K. Jörgensen, Optical-fiber temperature sensor based on upconversion-excited fluorescence, *Optics Letters*, Vol. 15, Issue 19, 1990, pp. 1100-1102.
- [13]. H. Fu, D. Chen, Z. Cai, Fiber Sensor Systems Based on Fiber Laser and Microwave Photonic Technologies, *Sensors*, Vol. 12, Issue 5, 2012, pp. 5395-5419.
- [14]. G. Liu, B. Jacquier, Spectroscopic properties of rare earths in optical materials, *Springer Science & Business Media*, 2006.
- [15]. D. J. Richardson, J. Nilsson, W. A. Clarkson, High power fiber lasers: current status and future perspectives, *Journal of the Optical Society of America B*, Vol. 27, Issue 11, 2010, pp. B63-B92.
- [16]. W. Blanc, B. Dussardier, Formation and applications of nanoparticles in silica optical fibers, *Journal of Optics*, Vol. 45, Issue 3, 2016, pp. 247-254.
- [17]. M. Vermillac, H. Fneich, J.-F. Lupi, J.-B. Tissot, C. Kucera, P. Vennégués, A. Mehdi, D. R. Neuville, J. Ballato, W. Blanc, Use of thulium-doped LaF₃ nanoparticles to lower the phonon energy of the thulium's environment in silica-based optical fibres, *Optical Materials*, Vol. 68, 2017, pp. 24-28.
- [18]. M. Vermillac, J. F Lupi, F. Peters, M. Cabie, P. Vennegues, C. Kucera, T. Neisius, J. Ballato, W. Blanc, Fiber draw induced elongation and break up of particles inside the core of a silica based optical fiber, *Journal of the American Ceramic Society*, Vol. 100, Issue 5, 2017, pp. 1814-1819.
- [19]. J. J. Kaufman, G. Tao, S. Shabahang, E. H. Banaei, D. S. Deng, X. Liang, S. G. Johnson, Y. Fink, A. F. Abouraddy, Structured spheres generated by an in-fibre fluid instability, *Nature*, Vol. 487, 2012, pp. 463-467.
- [20]. S. Xue, G. W. Barton, S. Fleming, A. Argyros, Analysis of capillary instability in metamaterials fabrication using fiber drawing technology, *Journal of Lightwave Technology*, Vol. 35, Issue 11, 2017, pp. 2167-2174.
- [21]. H. P. Grace, Dispersion phenomena in high viscosity immiscible fluid systems and application of static mixers as dispersion devices in such systems, *Chemical Engineering Communications*, Vol. 14, Issue 3-6, 1982, pp. 225-277.
- [22]. D. Kominsky, G. Pickrell, R. Stolen, Generation of random-hole optical fiber, *Optics Letters* Vol. 28, Issue 16, 2003, pp. 1409-1411.
- [23]. P. Tandon, M.-J. Li, D. C. Bookbinder, S. L. Logunov, E. J. Fewkes, Nano-engineered optical fibers and applications, *Nanophotonics*, Vol. 2, Issue 5-6, 2013, pp. 383-392.
- [24]. S. Karbasi, R. J. Frazier, K. W. Koch, T. Hawkins, J. Ballato, A. Mafi, Image transport through a disordered optical fibre mediated by transverse Anderson localization, *Nature Communications*, Vol. 5, 2014, 3362.
- [25]. B. Abaie, E. Mobini, S. Karbasi, T. Hawkins, J. Ballato, A. Mafi, Random lasing in an Anderson localizing optical fiber, *Light: Science & Applications*, Vol. 6, Issue 8, 2017, e17041.